In-vivo range verification in particle therapy

Katia Parodi and

Ludwig-Maximilians-Universität München, Department of Medical Physics, Am Coulombwall 1, Garching b. Munich, 85748 Germany

Jerimy C Polf

Deparment of Radiation Oncology, Maryland Proton Treatment Center, University of Maryland School of Medicine, 22 South Greene St., Baltimore, MD 21201, United States of America

Abstract

Exploitation of the full potential offered by ion beams in clinical practice is still hampered by several sources of treatment uncertainties, particularly related to limitations of our ability to locate the position of the Bragg peak in the tumour. To this end, several efforts are ongoing to improve the characterization of patient position, anatomy and tissue stopping power properties prior to treatment, as well as to enable in-vivo verification of the actual dose delivery, or at least beam range, during or shortly after treatment. This contribution critically reviews methods under development or clinical testing for verification of ion therapy, based on pre-treatment range and tissue probing as well as detection of secondary emissions or physiological changes during and after treatment, trying to disentangle approaches of general applicability from those more specific to certain anatomical locations. Moreover, it discusses future directions, which could benefit from integration of multiple modalities or address novel exploitation of the measurable signals for biologically adapted therapy.

1. INTRODUCTION

In the last years, radiation therapy with ion beams, especially proton beams, has been rapidly spreading worldwide. The interest in this advanced treatment modality lies in the favorable interaction properties of ion beams in matter, enabling concentration of a pronounced maximum of dose deposition in a localized region, so-called Bragg peak, which can be adjusted in depth by changing the initial beam energy[1]. This feature can enable a highly conformal dose delivery to the tumour with excellent sparing of critical organs and healthy tissue, thus promising possibilities of dose escalation for improved therapeutic outcome as well as reduced toxicity, a topic of increasing concern especially for the treatment of pediatric tumour[2]. Latest developments of advanced beam delivery based on pencil beam scanning (PBS, see Flanz et al in this special issue), in combination with the integration of volumetric imaging into the treatment room (see Landry and Hua in this special issue)

Katia.parodi@lmu.de.

Author Manuscript

further contributed to enhancing the achievable accuracy and precision of ion beam therapy at state-of-the-art treatment facilities.

Nevertheless, exploitation of the full potential offered by ion beams in clinical practice is still hampered by several sources of treatment uncertainties, particularly related to the finite ion beam range, determining the position of the Bragg peak. A major source of range uncertainty resides in the calibration of the diagnostic X-ray computed tomography (X-ray CT) images, acquired for treatment planning purposes, into ion beam range in tissue. To this end, efforts are ongoing to integrate dual-energy X-ray sources into the volumetric in-room image guidance, aiming to resolve ambiguities in effective atomic number and relative electron density by (possibly simultaneous) data acquisitions at two different X-ray spectra, as briefly discussed in the article by Landry and Hua of this special issue. Also, the use of energetic protons or heavier ion beams for radiographic/tomographic imaging of patient anatomy offers additional opportunities for probing patient tissue with the same radiation quality as used for therapy, to validate or even directly deduce the required stopping power information of tissue relative to water (stopping power ratio, SPR) for treatment planning.

Regardless of the correct characterization of patient position, anatomy and tissue stopping power properties prior to treatment, uncertainties still remain in the actual application of the intended dose, thus calling for additional methods for in-vivo assessment of the ion beam range or, ideally, dose delivery before, during or shortly after treatment[3]. Since the primary ions are stopped in the Bragg peak within the tumour, such in-vivo verification methods either must rely on pre-treatment low dose exposure with scouting fields, on detection of secondary emissions, or physiological changes induced by the therapeutic irradiation, measurable during or after treatment.

This contribution will thus review methods under investigation for in-vivo verification of ion beam therapy, based on pre-treatment range and tissue probing as well as detection of secondary emissions or physiological changes during and after treatment. Since some of the methods are of general applicability, while others are more specific to certain anatomical locations, a separation will be done between general-purpose techniques and those specific to certain sites.

2. GENERAL PURPOSE TECHNIQUES

2.A. Ion radiography and tomography

Radiographic (i.e., from one direction) or tomographic (i.e., from multiple directions) transmission of energetic ion beams through the body opens the possibility of imaging the patient with the same radiation quality and in the same position as for treatment. To date, most operational ion therapy facilities enable ion acceleration up to beam energies corresponding to approximately 30 cm penetration in water, which can be sufficient for imaging most of the anatomical locations of clinical interest in the head and upper abdomen[4]. Moreover, first commercial accelerator and beam delivery solutions (e.g., ProTom International, https://www.protominternational.com) exist, which intentionally target energies up to 330 MeV for the lighter proton beams, to overcome any possible restriction for transmission ion imaging especially in the pelvic area.

First efforts in ion based imaging date back to the pioneering investigations in the late 1960s, primarily aimed at low dose radiographic imaging at higher density resolution than with X-rays for radiologic applications[5]. Although potential applications to proton treatment planning were already envisioned in those early years[6], only in the last two decades the modality has attracted growing interest for providing information on the patient-specific tissue stopping power properties to reduce range uncertainties in ion beam therapy. Moreover, ion transmission imaging offers the possibility of assessing anatomical information in the treatment position and at lower dose than with conventional or emerging in-room X-ray image guidance, thus opening new perspectives for adaptive radiation therapy. According to Schulte et al[7], minimal requirements to be accomplished by ion computed tomography are a spatial resolution of 1 mm, a density resolution of 1%, an acquisition time of less than 5 minutes (besides a maximum of 10 min installation time) and a maximum dose of 5 cGy per scan, comparable to the nowadays used X-ray-CTs.

Most detector systems investigated so far for ion radiography and tomography rely on either monoenergetic[8–9] or properly energy-modulated[10–13] broad beams, covering a large irradiation area through passive scattering. However, experimental investigations exploiting PBS have also been reported[14–16]. Regardless of the considered ion species, the main proposed setups share the general concept of combining beam positional/directional information with residual energy or range measurement. However, considerable differences exist in the developed instrumentation, which can be classified according to the detection scheme aiming at either recording information for each individual beam particle, or integrating the signal resulting from the applied broad or narrow beam.

The most extensively investigated single particle tracking configuration relies on fast performing position sensitive detectors, e.g., scintillating fiber hodoscopes[8,14], gas-based electron multiplying detectors such as GEM (Gas-Electron-Multiplier)[17] or micromegas[18], or silicon strip detectors[7,18], placed before and after the imaging object. The tracking system is synchronized with the residual energy or range measurement in a single calorimeter[8] or a stack of detectors, such as plastic scintillators[14,17,19] (figure 1a) or even solid state detectors[20]. This way, a so called list mode of events is created, containing the individual ion entrance and exit positions (and possibly directions, depending on the number of tracking planes) with associated residual energy/range after the traversed object. These list mode data can be reconstructed with analytical[21,22] or iterative[23] algorithms, after proper filtering of events to remove particles having undergone nuclear interactions or too large angular deflection. Coulomb scattering is in general an issue, especially challenging the achievable spatial resolution with the lighter proton beams. In this case, the complete tracking information of particle position and direction before and after the object is typically used to estimate the most likely path of individual ion trajectories, thus enabling to account for the particle curved paths in the image reconstruction process[21]. In addition to the complexity and cost of the detection system, high demands are posed on the system electronics, which has to handle MHz of events at typical irradiation conditions of broad beams[7].

For the less scattering carbon ions delivered with PBS techniques, the center of gravity of each pencil beam can be extrapolated from the measurement of position sensitive detectors permanently installed in the beam nozzle, thus simplifying the acquisition setup, e.g. limited

to a residual range measurement in Rinaldi et al[15] (figure 1b). When trading the capability of single ion detection for the sake of simplicity and cost-effectiveness of the detector system, the residual energy or range measurement can be pursued with multi-layer dosimetric systems, e.g., based on a stack of large-area plane-parallel ionization chambers interleaved with passive absorbers[15,25] (figure 1b). Such systems aim at identifying the Bragg peak position from the acquired laterally integrated depth dose curves. The major limitation of this approach is that in presence of tissue heterogeneities perpendicular to the beam direction the measured Bragg curve integrates information related to the different ion paths in different tissue, depending on the pencil beam initial spot size and in-tissue scattering. On the other hand, advanced data processing techniques may enable disentangling the mixed residual range information[26,27] and properly rearrange it spatially[26], showing promising results also in the case of the more scattering proton beams, when combined to prior X-ray information[26].

While the usage of monoenergetic passively scattered or scanned beams simplifies the data acquisition and processing, it typically results in bulky detection systems, depending on the detector solution used for the residual beam energy or range measurement. Hence, alternative approaches have suggested the replacement of calorimeters or range telescopes with thinner detection systems for space-resolved energy loss or fluence measurements, e.g. via a combination of a scintillation screen and charge-coupled device camera or flat panel/array detectors. However, due to remaining ambiguity for data interpretation, these measurements after the traversed tissue are typically performed for polyenergetic irradiation, obtained either with quasi-simultaneous superposition of different beam energies and fluences e.g., created by means of modulation wheels, or sequential irradiation with monoenergetic beams of different energies, as adjusted with corresponding active energy variation or passive degradation. Examples of such systems were reported by Zygmanski et al[10] and Ryu et al[28] for proton beams, as well as in Abe et al[11], Muraishi et al[12] and Telsemeyer and al[16] for carbon ion beams. Despite the simplification and cost-effectiveness of the setup, together with the excellent spatial resolution of the typically employed planar detector systems, unavoidable limitations in image quality were encountered especially due to Coulomb scattering for the lighter protons[10]. An additional possibility in case of passive energy variation with a range modulation wheel is to encode the water equivalent thickness of the traversed tissue in the time pattern of the dose signal acquired by a fast detection system, such as a diode-array capable of fast dose rate measurements at ~100 ms resolution[24] (figure 1c). However, due to the need of a passively scattered beam with a range modulator, this method is not applicable to the majority of modern facilities equipped with PBS delivery only.

Although no clinical device of ion transmission imaging is existing yet, very encouraging simulation studies and experimental campaigns with the available prototypes confirm the promise of this modality, approaching the original specifications of Schulte et al 2004[7]. In particular, their second-generation system[9,29] was shown able to provide an SPR accuracy of 1% for different medium-size (head-like) objects at an imaging dose of about 1.5 mGy and a spatial resolution between 5 and 8 line pairs per cm at 10% of the modulation transfer function in full proton scans of less than 7 min[19,30]. For these investigations, imaged objects featured cylindrical phantoms with experimentally characterized tissue equivalent inserts as

well as a pediatric head phantom[30] (figure 2). Further dose reduction possibilities could be achieved by exploiting the unique flexibility offered by PBS to properly modulate and increase the ion beam fluence in pre-defined anatomical regions of interest, while keeping radiation dose low in less interesting anatomical parts not relevant for treatment planning[31]. Moreover, several groups have demonstrated that single radiographic projections based on actual ion residual energy/range measurements, combined with prior X-ray CT images, could be sufficient to refine and personalize the Hounsfield Units (HU)-range calibration curve[26,32]. Similarly, range probing of only a few transmitted pencil beams could offer an attractive low dose pre-treatment check, able to provide information on corrective actions (e.g., positional changes) prior to treatment[33]. Additional few studies addressed the possibility to use the different dependences of beam attenuation and scattering in the traversed object to complement energy loss information for improved tissue characterization[34,35]. While the investigations were so far mainly focused on the clinically available proton and carbon ion beams, recent studies have started addressing, both theoretically and experimentally, the potential of other ion beams being (re)considered for clinical introduction in the near future, particularly given the independence of the SPR needed for treatment planning on the imaging ion species. In this respect, helium ions are regarded as a very promising candidate, owing to their reduced lateral scattering compared to protons, and reduced imaging dose (at the same image quality) compared to carbon ions[36–39]. In particular, Volz et al[38] confirmed experimentally almost a factor of two increased spatial resolution of ^{4}He ion radiography compared to proton radiography, as acquired with the same second generation prototype of refs.[9,29]. However, no dose information was provided, and encountered experimental difficulties challenged the quality of the obtained tomographic data[38]. Regardless of the ion species, but depending on the beam delivery capability as well as detector efficiency and data acquisition speed, it could be foreseeable to extend the technology to intra-fractionally moving targets for very fast radiographic imaging of minimal dose, similar to fluoroscopy[40]. This approach could enable verifying the integral SPR in specific motion states at least in few regions of interest to confirm treatment planning predictions based only on anatomical information for reliable motion-mitigated particle therapy (cf. Mori et al of this special issue).

Summarizing, ion radiography and tomography have not yet reached the stage of clinical application. However, from the current rapid progress it can be expected that the next years will see the transition of first imaging prototypes to pre-clinical and hopefully clinically testing with protons and even heavier ion species, eventually aiming to improve the pre- (maybe even intra-) treatment patient model and related range prediction for improved treatment planning and adaptive strategies.

2.B. Positron-Emission-Tomography

Positron-Emission-Tomography (PET) imaging via detection of the coincident, antiparallel 511 keV photon pairs following the annihilation of the positron emitted in the β+-decay of neutron deficient nuclei has been the most extensively clinically investigated method for non-invasive, in-vivo visualization of the delivered ion treatment. Following a pioneering clinical investigation for pituitary ablation therapy with transmitted Helium ion beams[41] almost 50 years ago at the Lawrence Berkeley National Laboratory, the technique was

further attempted mostly in a pre-clinical setting for low-dose pre-treatment imaging of implanted β^+- radioactive ion beams (e.g., ^{19}Ne) prior to the therapeutic irradiation with the stable isotope species (e.g., ^{20}Ne)[42].

Besides the major challenge to produce high intensity radioactive beams, which is nowadays being tackled again especially at facilities able to offer so called post-acceleration[43], it was already understood that a minor amount of β^+-active nuclides is also produced through nuclear fragmentation reactions in tissue as a by-product of the irradiation[41,44]. The resulting activity pattern and its correlation with the dose delivery strongly depends on the primary ion species and the underlying projectile (for Z >1) or target fragmentation mechanism. In particular, heavy ions (Z ≥5) typically produce a β^+-activity signal with a peaked maximum located shortly before the Bragg peak, originating from positron emitting projectile fragments of the same charge but lower weight than the primary ion beam (e.g., ^{11}C from ^{12}C). On the other hand, target fragmentation is responsible for a track of activation all along the beam penetration depth, sensitive to the elemental tissue composition (e.g., ^{15}O from neutron stripping of ^{16}O tissue nuclei) and ceasing a few millimeters before the Bragg peak, depending on the medium stopping power properties and the energy threshold for nuclear reaction. This different formation process results in a stronger spatial correlation of the β^+-activity induced by heavy ion (e.g., ^{12}C) irradiation with the dose delivery, at the expense of a typically weaker PET signal compared to lighter ions (e.g., protons) at the same clinical (i.e., taking relative biological effectiveness into account[2]) fraction dose[45,46]. Owing to the typical half-lives ranging from few milliseconds up to tens of minutes (e.g., approximately 20 min for ^{11}C and 2 min for ^{15}O), the irradiation-induced β^+-activity can be detected during or after the therapeutic irradiation.

To this end, the unconventional application of PET to ion therapy monitoring could rely on direct usage or adaptation of existing technology well established for clinical and pre-clinical nuclear medicine imaging. In particular, clinical experience reported so far was based on dedicated instrumentation integrated in the beam delivery, featuring dual-head in-beam[47] and on-board[48] systems, a neurological full-ring scanner on-wheel moved to the treatment room at the end of irradiation[49], and commercial nuclear medicine full-ring PET scanners, nowadays typically combined with Computed Tomography (CT), installed in a nearby room[50–51] (figure 3). The latter so called offline workflow typically requires long acquisition times up to 30 min to compensate for the loss of a major fraction of the produced activity in the time elapsed between irradiation and imaging, due to physical and physiological (e.g., blood transport) decay. For data interpretation, it should be kept in mind that the PET signal is due to secondary emissions induced by nuclear reactions. Hence, it can only be correlated to but not identical to the therapeutic dose delivery and beam range, which are mainly due to electromagnetic interactions. Therefore, the verification process entails the comparison of the reconstructed PET image with an expectation obtained either from a Monte Carlo[52–54] or an analytical[55–57] model of the treatment delivery and image formation process, or a reference measurement from a previous treatment fraction[48] (figure 4).

Initial clinical results relying on either of the above mentioned in-beam, in-room and offline imaging workflows showed the capability of the method to detect inter- (and in some cases

even intra-) fractional anatomical changes or positioning errors with different ion beams and PET scanners[48,49,58–64]. For in-beam/on-board instrumentation a detailed quantitative range analysis for clinical data was not reported. In-room PET scans of 20 min typically starting within 3 min after passively scattered proton therapy were challenged by co-registration errors of approximately 2 mm, causing average range differences within 5 mm (even < 3 mm for 6 out of 8 patients) for the investigated cranial lesions, with similar results obtained for the first 5 min of acquisition[60]. For the less optimal offline implementation with 30 min acquisition typically started within 10 min after PBS proton and carbon ion delivery, reproducibility between treatment sessions typically better than 1mm was reported for head indications[63,64]. When comparing to MC calculations on the planning[62–64] or properly calibrated PET/CT CTs[62], agreement within 2–5 mm for different locations was reported, with better results especially achieved for cranial tumour indications, which allow for more reproducible fixation and reduced washout in bony structures. In case of inter-fractional changes, shifts up to ±3mm could be deduced from both PET measurements and simulations, and found well correlated (typically within 1.8mm) to anatomical changes derived from repeated CT scans, in agreement with dose data[62]. However, the method turned out to be challenged by several limiting factors such as image quality for the encountered counting statistics, which were orders of magnitude below conventional tracer imaging, co-registration issues especially for extra-cranial sites subject to organ motion, and physiological washout, especially pronounced for offline workflows[3,62].

While these limitations could be disentangled and taken into account in the data evaluation process with corresponding uncertainty maps to support decision making[63], most of them can be actually attributed to the so far practiced adoption of sub-optimal instrumentation for the sake of fast clinical translation. Part of this problem is due to the high costs of PET detectors and the small market of ion therapy, which discouraged industrial support and prompted only a few selected research-oriented institutions to pursue their investigations using or adapting instrumentation originally designed for higher statistics nuclear medicine or small-animal imaging. Nevertheless, new efforts specifically tailored to the problem of range monitoring in ion beam therapy have been undertaken over the last years. These initiatives resulted in the realization of new generation in-beam PET scanners based on either limited angle dual-head designs[65] or special full-ring arrangements, featuring a dual-ring as well as a slanted or axially-shifted single-ring configuration[66–68] leaving an opening for the beam and the patient. The latter special full-ring geometrical arrangements were made possible by the progress in depth-of-interaction PET detectors, enabling the exploitation of oblique lines of response while preserving acceptable image quality. Along with the geometrical design optimization tailored to the special needs of ion beam therapy, the new systems also offer improved data acquisition features such as the ability to record usable data during the actual beam-on time, despite the considerable production of background radiation[69,70]. Moreover, advancements in fast image reconstruction algorithms on graphical processing units can already enable dynamic visualization of the irradiation-induced activity during the beam delivery, at a typical resolution of tens of seconds as mostly constrained by the accumulation of sufficient counting statistics. Ongoing developments in PET detectors and photo-sensors can further open the perspective of on-the-fly reconstruction due to their ultrafast time performanc[71]. Some groups are also considering

utilization of the very short-lived (~ms) positron emitters produced during irradiation, such as ^{12}N[72], to overcome the major drawback of PET as an intrinsically delayed (with respect to the beam delivery) imaging technique.

Some of the above described new generation systems have already entered the phase of clinical testing, while others are expected to find translation into clinical trials in the coming year(s). The resulting data will allow drawing new insights on the role of PET for in-vivo treatment verification, in comparison to the reviewed clinical experience with the not yet optimized systems, as well as the first clinical tests reported for emerging new modalities such as prompt gamma imaging (see next section).

2.C. Prompt gamma

An alternative to PET imaging for range verification is to detect prompt gammas (PG) emitted during inelastic interactions of the incident protons or heavier ions with nuclei in the irradiated tissues. The imaging of PG emission was first suggested by Stichelbaut and Jongen[73], and has garnered increasing interest as a range verification technique. PGs are emitted when a nucleus is first excited during a scattering event with a proton (ion) which may then emit characteristic photons (whose energy depends on the type of elemental nuclei involved) during its cascade through various energy levels as it returns to the ground state. This emission occurs immediately (within nanoseconds) after proton-nucleus scattering, and was shown in initial measurements[74,75] to correlate well with the depth dose profile of therapeutic proton and carbon ion beams. The results of these first measurements led to several initial Monte Carlo based studies of spatial distributions of PG emission from tissue during delivery of primarily proton radiotherapy beams[76,77], which showed a strong correlation with the dose delivery.

The success of the initial measurements and Monte Carlo studies have led many research groups to work on the development of prompt gamma range verification systems. Since the range of PG energies emitted from tissue (2 MeV – 10 MeV) are above those typically used in diagnostic and nuclear medicine studies (< 1 MeV), a large effort has been put forth into the development of detection systems that can measure the spatial distribution of PG emission during the delivery of a proton treatment. Such systems include so-called knife-edge slit and multi-slit collimated cameras, fast scintillators, and multi-stage Compton cameras.

The slit camera consists of an array of gamma detectors aligned behind a tungsten or lead collimator containing a single knife edge slit[78], as shown in Figure 5. The knife-edge slit is aligned perpendicular to the beam central axis, and the PGs passing through the slit in the collimator are measured to produce a one-dimensional profile of the PG emission along the beam path[79–81]. Different slit camera verification systems employ different background suppression methods, such as closed-collimator background subtraction[82] or energy and time-of-flight detection systems[83,84] to help improve the cameras ability to localize the distal fall-off to the PG profile. Such camera has shown the ability to measure shifts in proton beam Bragg peaks under clinical conditions, and results of its initial clinical application for in vivo range monitoring during proton radiotherapy treatment delivery for tumours in the head have recently been reported[85,86]. As seen in Figure 6[86], two-

dimensional range maps of each spot in each energy layer delivered for a given treatment field can be produced. These maps can give a visual representation of the change in measured range from what was calculated by the treatment plan for each spot for any given treatment fraction. For the relatively homogenous brain anatomy considered in this study, a range shift retrieval precision of 2 mm was found when aggregating the prompt gamma signal from neighbouring spots to increase counting statistics, however mostly limited by the positioning accuracy of the trolley system.

Two types of fast scintillator based systems have been developed for range verification, as shown in Figure 7; energy-time resolved prompt gamma spectroscopy (PGS)[87] and prompt gamma timing systems (PGT[88]), shown in Figure 7. For PGS, a collimated fast-scintillator is used to measure the energy spectrum and time-of-flight of PG emission during irradiation. Each discrete PG emission energy emitted from irradiated nuclei has a unique correlation to the proton dose delivery due to the differing nuclear reaction cross-sections as a function of proton energy[84]. These differences in PG emission rate can be used as prior knowledge, which Verburg et al[90] showed to be feasible for deducing proton beam range from PG emission spectra measured at fixed points along the proton beam path. This technique has undergone testing over a wide range of clinical-like scenarios[90–92], and initial clinical trials of PGS based range verification during patient treatment are expected to begin soon.

In addition, PGT uses several uncollimated fast scintillator detectors positioned around the patient and measures the difference in time from the exit of the proton beam from the treatment delivery nozzle and the detection of the PGs by the scintillators. As the range of the beam in the patient changes, both the time it takes the proton to traverse the patient and the time for the gamma to travel to the detector increase. Studies have shown[88,93] that the properties of the measured PG timing profile are directly correlated to the proton range in the patient, and thus provide a method to measure the in vivo range of the delivered treatment beam. Based on the results of initial studies of this method, researchers are now investigating methods to integrate PGT within the clinical beam acceleration and treatment delivery workflow, as well as its viability over a wider range of clinical proton therapy scenarios[94].

Another detector being developed for PG based range verification is the Compton camera (CC). The CC, as originally proposed for medical imaging by Todd et al[95], consists of two or more detector stages in which a gamma ray may interact as it passes through the CC. By recording the position and energy deposited by a PG that Compton scatters in one CC stage and then interacts in another stage (Compton scatter, photoelectric absorption, pair productions) it is possible to use the Compton scattering formulas to determine a "cone-of-origin" for the PG as illustrated in Figure 8. Based on the physics of Compton scattering, we know that the PG must have originated somewhere on the surface of the cone-of-origin. By then backprojecting the origin-cone through space an image of the PG emission can be constructed. Many researchers have studied the design of CCs for imaging of PG emission during proton therapy. This includes Monte Carlo studies to understand the achievable spatial and energy resolution for two and three stage CCs, and to determine the effect these limitations have on detection efficiency and achievable image resolution[96–99]. Additionally, many studies of CC designs specifically for PG based range verification have been

performed, including size/shape studies to optimize detection efficiency[98–101], studies of secondary particle and background interactions in the CCs on final image noise[102], and studies of new types of detectors to improve detection efficiency and reduce noise in the final reconstructed image[96,98,103–107]. Several research studies have also focused on the development of new image reconstruction techniques to improve the spatial resolution of images of PG emission taken with a CC. The most prominent techniques include the use of statistical algorithms that iteratively determine an estimate of the number of PGs emitted per image voxel that were detected during delivery of a particle therapy beam[96,98,108,109].

Several prototype CCs have been constructed and tested in clinical proton therapy environments[110–113]. As shown in Figure 8, one such design currently being tested consists of a two-stage CC mounted on the underside of the treatment couch. This would allow the CC to be moved in the patient superior-inferior direction (along the underside of the couch) to align with the location of the treatment site within the patient. The ability to produce 3D images and detect shifts in the beam range as small as 3 mm with clinical treatment beams with this prototype system was recently demonstrate by Draeger et al[114]. With continued development, these systems are expected to begin pre-clinical testing and characterization, with initial clinical trials for CC based range verification to begin soon after in the coming year(s).

Summarizing, many features of the characteristic prompt gamma (spatial distribution, energy, time) can be utilized for range monitoring and beyond (e.g., tissue characterization), and several prototypes of corresponding detection systems have been realized, with first promising clinical testing so far reported for passively scattered and PBS proton irradiation of cranial lesions.

3. TECHNIQUES SPECIFIC TO CERTAIN ANATOMIC SITES

Several range and dose verification solutions tailored to specific anatomic sites have also been studied. This includes studies of fiducial markers that contain a MOSFET dosimeter and a wireless transmitter for real-time communication of dose delivery in phantom based studies of prostate and brain cancer treatments[116–117]. These wireless dosimeters showed a dose determination accuracy of 5% in the anthropomorphic phantom tests[116]. Also, Lu et al reported on a method to predict the residual range of the beam beyond the point of the implanted MOSFET using sloped spread out Bragg peaks[117]. Additionally, the use of fiducials in which positron emitters are produced during proton irradiation was reported by Cho et al[118]. Here, the long-lived positron annihilation gamma activity induced in selected materials was proposed for imaging post treatment, in comparison to expected activity levels based on the planned dose delivery. These devices only provide information about beam intensity at the point in the body where they are located, and in cases of specially designed dose delivery schemes, can accurately predict the remaining range of the beam beyond the implanted dosimeter ~50% of the time[117]. With x-ray therapy these devices have been employed to provide point dose measurements for validation of treatment delivery. If assessment of dose delivered at a single point is desired, then these devices have been shown to be adequate in ion beam therapy[118]. However, if an assessment of the in vivo beam range is desired, then the measurement of at least 1D dose profile or some other parameter (such as

intensity or ratios of prompt gamma emission lines) is needed to assess where the beam stops in the patient. Additionally, if the implanted dosimeters are placed near the end of the beam range, there is concern that they could themselves cause a clinically significant perturbation of the beam range. So a single point dose measurement as provided by implanted fiducials or wireless dosimeters is not adequate for assessment of in vivo beam range.

As another solution for prostate therapy, a diode detector array implanted within a rectal balloon can be inserted and aligned along the rectal wall[119–122]. Initial studies of such an array showed that with the delivery of an initial scout dose that purposely ranges into the rectal balloon, the water equivalent path length (WEPL) of the beam can be deduced from changes in the dose pattern that occur during delivery of passively scattered proton beams[120, 122]. The determined WEPL can then be applied to calculation of the full treatment dose to determine its range for that particular treatment fraction. This approach can provide a verification that the beam range through the anatomy and current bladder filling matches that of the treatment plan before the full treatment field is delivered.

In addition, preliminary studies showed that it is possible to visualize the beam range from changes in the appearance of spine and liver tissues on follow up MRI images[123,124]. These studies have shown the feasibility of using MR imaging as method assessing treatment delivery for follow up studies conducted after completion of the treatment course. Current challenges include determination of the onset time of visible irradiation-induced physiological changes, their correlation to the beam range, and the confounding effects of inter-patient variability.

Another interesting signature reported for the first time in the case of liver treatment is related to thermoacoustic emissions, following the ion energy deposition in tissue and the resulting localized heating. This signal, nowadays referred to as protoacoustics or ionoacoustics, could be detected in the 1990s by a broadband hydrophone placed on the patient skin during passively scattered proton treatment at a specially pulsed synchrotron[125]. However, this scenario was challenged by the unfavorable setting of passive beam delivery, resulting in a complex signal of difficult interpretation. The past few years have seen a renewed interest in this technique. In fact, acoustic emissions strongly depend on the concentration of energy deposition in space and time. Hence, current trends of pencil-beam scanning and intrinsically pulsed compact synchrocyclotron proton accelerators (emerging in the context of single-room proton therapy facilities) offer ideal conditions of a well-localized energy deposition pattern on a favorable time scale of a few microseconds high-intensity (~pC) pulses, thus maximizing the measurable acoustic emission, particularly pronounced at the Bragg peak[126,127]. In water, two independent studies recently reported the feasibility of (sub)millimetre range resolution for single pencil beams produced at either an intrinsically (synchrocyclotron[128]) or an artificially (isochronous cyclotron[129]) pulsed proton accelerator, when delivering a dose of a few Gy, comparable to levels applied in typical hypofractionated treatment schemes. Although tissue heterogeneities increase signal attenuation and distort its shape, simulations studies still support the feasibility of achieving millimetre range accuracy in selected anatomical locations of favourable acoustic accessibility, when using multiple detectors of enhanced sensitivity and proper triangulation

techniques[130,131]. Along with the possible combination with anatomical ultrasound imaging[132,133], this technology represents a very promising and cost-effective mean for in-vivo range (and possibly also dose) verification of several envisioned anatomical sites such as prostate, liver and breast[126], where precision treatment delivery is currently challenged by inter- and intra-fractional organ motion.

Summarizing, MRI imaging has already been applied to visualization of physiological changes correlated to the beam range in follow-up investigations after completion of the entire proton therapy treatment course for craniospinal and liver tumours. Other techniques especially relying on multiple time-resolved dose measurements or triangulation of acoustic signals generated at the Bragg peak are currently under investigation for possible future translation especially to passively scattered and PBS techniques, respectively, for prostate and, in the latter case, other locations of sonic accessibility.

4. SUMMARY AND OUTLOOK

In the last decade(s), several techniques have been proposed and explored in the context of in-vivo range monitoring, in order to counteract one of the remaining major sources of uncertainty for full clinical exploitation of the ballistic tumour-dose conformality offered by modern ion beam therapy. Although no routine solution has been established yet and only few clinical experiences have been reported for PET, prompt gamma, MRI and even one isolated attempt of ionoacoustics, several prototype systems tailored to the specific needs of ion beam therapy have been realized over the last few years and are just entering or are about to enter clinical testing. While the next years will likely see the maturing and growing adoption of proven technologies, it is foreseeable that none of them will offer alone the ultimate solution to the problem of range uncertainty and other possible applications, thus requiring their integration into the treatment workflow and maybe even their combination. Depending on the costs and flexibility of the detector systems, different solutions might also be adopted for different beamlines at multiroom treatment facilities.

On-target radiographic and/or tomographic ion transmission imaging prior to the treatment will likely be regularly employed to provide updated patient anatomical information with accurate (integral) SPR determination for pre-treatment verification and potential treatment adaptation, either alone or in combination with additional diagnostic or on-site X-ray imaging (cf. paper of Landry and Hua in this special issue). Depending on the anatomical location and established clinical workflows, such pre-treatment transmission ion imaging might be complemented by dosimetric assessment or range probing of selected pencil beams or scout fields in selected regions of interest based on implanted dosimeters or fiducials.

In addition to these measures aimed at a pro-active corrective strategy prior to the delivery of the entire fraction dose, many centers will likely adopt in-situ range verification techniques exploiting secondary emissions based on nuclear reaction processes (PET, prompt gamma) or thermoacoustic effects (ionoacoustics). While the former can provide a generally applicable method not restricted to a specific anatomical location, ionoacoustics will be limited to sites of suitable sonic access, however providing the potential advantage of a compact and cost-effective solution lending itself to intra-modality co-registration with

additional ultrasound imaging for real-time verification of the beam range and patient anatomy. In terms of PET and PG verification, the experience to be generated with new dedicated devices just entering clinical testing in few selected centers will enable drawing a more definitive conclusion on their accuracy and reliability for different treatment sites. Moreover, it will enable identifying the best approaches for using the PET or PG information for reactive corrective strategies during treatment (e.g., interruption of irradiation and ideally on-the-flight adaptation) or prior to the next treatment fraction.

Since it is not unlikely that each technique will show its strength and superiority in some particular scenario, concepts aiming at the synergistic combination of both PET and PG modalities have also been proposed and are under design optimization for future envisioned development[134]. Availability of PET at the treatment site might not only provide intrinsically volumetric imaging modalities to complement real-time 1D prompt gamma range verification, but also open additional perspectives of biological imaging. Such volumetric imaging methods could provide e.g. new insights on special tumour sub-regions (e.g., hypoxic areas) to be precisely targeted with escalated doses or more effective radiation qualities, and enable time-resolved, direct tumour tracking. With the future development of specific molecular targeting agents, these methods could be used to visualize and map specific radiation damage mechanisms as a means to link to dLET and RBE models for image- and biologically-guided adapted therapy. However, feasibility of such approaches will depend on the progress of both improved in vivo PET as well as molecular imaging and biomarker developments, along with logistic considerations for external tracer injection.

Alternatively, new frontiers might be explored in relation to the already mentioned spectroscopic capability of PG imaging. In fact, each element in tissue emits a unique spectrum of PGs during proton irradiation[135–137]. In addition to the already reported use of the best emission lines for range verification[74,76, 87, 89, 111,113], it has also been shown that the total emission from oxygen per unit dose is directly proportional to the concentration of oxygen within a proton beam irradiated volume of tissue[138]. This observation led to suggestions that if PG emissions from several key elements in tissue (O, C, N, Ca, etc.) could be accurately determined as a function of dose per volume, then spectroscopic PG imaging could be used to determine the composition and concentration of these key elements in tissues, such as oxygen[138]. As illustrated in Figure 9, If elemental concentration in the irradiated tissues could be imaged on a daily basis over the course of a treatment, it could provide information about tumour response (such as changing hypoxia levels), which could inform and help Oncologists better adapt treatment delivery based on each patient individual response to treatment.

In addition to on-site PET and PG imaging or, for specific indications, ionoacoustic/ ultrasound monitoring, post-treatment MR images showing irradiation-induced physiological changes might also be used to provide additional insights on both the beam range and treatment response. Ideally, such transformations could be already detectable during fractionated therapy for individualized feedback to the patient-specific treatment course, rather than assessment of patient-population characteristics. In this respect, the envisioned integration of MR imaging into the ion therapy beam delivery[139] might simplify the workflow for such regular MR investigations. Moreover, availability of updated patient

anatomical information during treatment with MRI-guidance would open new avenues in the management of treatment uncertainties. This would especially apply to the challenging cases of moving tumours (cf. Knopf et al in this special issue) for which all above discussed techniques are in principle applicable, especially those offering real-time capabilities, but for which further developments and carefully testing are still needed.

Concluding, much progress in the context of advanced imaging and in-vivo verification of ion beam therapy has been jointly pursued by several academic, industrial and clinical groups worldwide. However, a lot of work remains to be done to identify and in some cases even combine the most promising approaches and enable their translation and integration into the clinical workflow, eventually aiming to defeat the yet unmet challenge of range uncertainty for full exploitation of the physical advantages of ion beams in clinical practice.

Acknowledgments

References.

1. Wilson RR. Radiological use of fast protons. Radiology 1946; 47(5):487–91. [PubMed: 20274616]

2. Durante M and Loeffler JS. Charged particles in radiation oncology. Nat Rev Clin Oncol 2010;7(1): 37–43. [PubMed: 19949433]

3. Knopf AC and Lomax A. In vivo proton range verification: a review. Phys Med Biol 2013; 58: R131–60. [PubMed: 23863203]

4. Rinaldi I, Brons S, Jäkel O et al. Investigations on novel imaging techniques for ion beam therapy: carbon ion radiography and tomography. IEEE NSS/MIC Conference Record 2011; MIC11–3: 2805–10.

5. Koehler AM. Proton radiography. Science 1968;160: 303–4. [PubMed: 17788234]

6. Cormack AM. Representation of a Function by Its Line Integrals, with Some Radiological Applications. J Appl Phys 1963; 34:2722–27.

7. Schulte R, Bashkirov V, Li T, et al. Design of a Proton Computed Tomography System for Applications in Proton Radiation Therapy. IEEE Trans Nucl Sci 2004; 51: 866–72.

8. Shinoda H, Kanai T and Kohno T, Application of heavy-ion CT, Phys Med Biol 2006; 51: 4073–81. [PubMed: 16885625]

9. Sadrozinski HFW, Geoghegan T, Harvey E et al. Operation of the preclinical head scanner for proton CT. Nucl Instrum Meth A 2016; 831:394–9.

10. Zygmanski P, Gall KP, Rabin MS and Rosenthal SJ. The measurement of proton stopping power using proton-cone-beam computed tomography. Phys Med Biol 2000; 45: 511–28. [PubMed: 10701518]

11. Abe S, Nishimura K, Sato H et al. Heavy ion CT system based on measurement of residual range distribution. Igaku Butsuri 2002; 22:39–47. [PubMed: 12766295]

12. Muraishi H, Nishimura K, Abe S, et al. Evaluation of Spatial Resolution for Heavy Ion CT System Based on the Measurement of Residual Range Distribution With HIMAC. IEEE Trans Nucl Sci 2009; 56:2714–21.

13. Zhang R, Jee KW, Cascio E, Sharp GC, Flanz JB, Lu HM. Improvement of single detector proton radiography by incorporating intensity of time-resolved dose rate functions. Phys Med Biol 2017;63:015030. [PubMed: 29116055]

14. Schneider U, Besserer J, Pemler P et al. First proton radiography of an animal patient. Med Phys 2004; 31: 1046–51. [PubMed: 15191291]

15. Rinaldi I, Brons S, Jäkel O et al. Experimental investigations on carbon ion scanning radiography using a range telescope. Phys Med Biol 2014; 59: 3041–57. [PubMed: 24842455]

16. Telsemeyer J, Jäkel O and Martišíková M. Quantitative carbon ion beam radiography and tomography with a flat-panel detector. Phys Med Biol 2012; 57: 7957–71. [PubMed: 23154641]

17. Bucciantonio M, Amaldi U, Kieffer R at al. Development of a fast proton range radiography system for quality assurance in hadrontherapy. Nucl Instrum Methods Phys Res Sect A 2013; 732: 564–7.

18. Dolney D, Ainsley C, Hollebeek R, Maughan R. Monte Carlo simulations of a novel Micromegas 2D array for proton dosimetry. Phys Med Biol 2016; 61(4):1563–72. [PubMed: 26816338]

19. Plautz T E, Bashkirov V, Giacometti V et al. An evaluation of spatial resolution of a prototype proton CT scanner. Med Phys 2016; 43: 6291–300. [PubMed: 27908179]

20. Poludniowski G, Allinson N M, Anaxagoras T, et al. Proton-counting radiography for proton therapy: a proof of principle using CMOS APS technology. Phys Med Biol 2014; 59: 2569–81. [PubMed: 24785680]

21. Rit S, Dedes G, Freud N, Sarrut D and Letang JM. Filtered backprojection proton CT reconstruction along most likely paths. Med Phys 2013; 40: 031103. [PubMed: 23464283]

22. Poludniowski G, Allinson NM and Evans PM. Proton computed tomography reconstruction using a backprojection-then-filtering approach. Phys Med Biol 2014; 59: 7905–18. [PubMed: 25426839]

23. Penfold SN, Schulte RW, Censor Y, Rosenfeld AB. Total variation superiorization schemes in proton computed tomography image reconstruction. Med Phys 2010; 37: 5887–95. [PubMed: 21158301]

24. Testa M, Verburg JM, Rose M et al. Proton radiography and proton computed tomography based on time-resolved dose measurements. Phys Med Biol 2013; 58: 8215–33. [PubMed: 24200989]

25. Farace P, Righetto R and Meijers. A Pencil beam proton radiography using a multilayer ionization chamber. Phys Med Biol 61; 2016: 4078–87. [PubMed: 27164479]

26. Krah N, Testa M, Brons S et al. An advanced image processing method to improve the spatial resolution of ion radiographies. Phys Med Biol 2015; 60: 8525–47. [PubMed: 26485618]

27. Meyer S, Gianoli C, Magallanes L, et al. Comparative Monte Carlo study on the performance of integration- and list-mode detector configurations for carbon ion computed tomography. Phys Med Biol 2017; 62: 1096–112. [PubMed: 28092630]

28. Ryu H, Song E, Lee J, Kim J. Density and spatial resolutions of proton radiography using a range modulation technique. Phys Med Biol 2008; 53:5461–8. [PubMed: 18765893]

29. Johnson RP, Bashkirov V, DeWitt L et al. A Fast Experimental Scanner for Proton CT: Technical Performance and First Experience With Phantom Scans. IEEE Trans Nucl Sci 2016; 63: 52–60. [PubMed: 27127307]

30. Giacometti V, Bashkirov VA, Piersimoni P et al. Software platform for simulation of a prototype proton CT scanner. Med Phys 2017; 44:1002–1016 [PubMed: 28094862]

31. Dedes G, De Angelis L, Rit S et al. Application of fluence field modulation to proton computed tomography for proton therapy imaging 2017. Phys Med Biol 2017; 62: 6026–43. [PubMed: 28582265]

32. Doolan PJ, Testa M, Sharp G et al. Patient-specific stopping power calibration for proton therapy planning based on single-detector proton radiography. Phys Med Biol 2015; 60: 1901–17. [PubMed: 25668437]

33. Mumot M, Algranati C, Hartmann M et al. Proton range verification using a range probe: definition of concept and initial analysis. Phys Med Biol 2010; 55: 4771–82. [PubMed: 20679697]

34. Bopp C, Colin J, Cussol D et al. Proton computed tomography from multiple physics processes. Phys Med Biol 2013; 58: 7261–76. [PubMed: 24076769]

35. Quinones CT, Letang JM and Rit S. Filtered back-projection reconstruction for attenuation proton CT along most likely paths. Phys Med Biol 2016; 61: 3258–78. [PubMed: 27032330]

36. Hansen DC, Bassler N, Sorensen TS and Seco J. The image quality of ion computed tomography at clinical imaging dose levels. Med Phys 2014; 41: 111908. [PubMed: 25370641]

37. Kopp BMG, Ion Imaging with Protons, Helium- and Carbon Ions: An experimental study, Master Thesis, LMU Munich, 2017.

38. Volz L, Collins-Fekete CA, Piersimoni P et al. Stopping power accuracy and achievable spatial resolution of helium ion imaging using a prototype particle CT detector system. Curr Dir Biom Eng 2017; 3: 401–404.

39. Gehrke T, Gallas R Jäkel O, Martišíková M. Proof of principle of helium-beam radiography using silicon pixel detectors for energy deposition measurement, identification, and tracking of single ions. Med Phys 2017 doi: 10.1002/mp.12723. [Epub ahead of print].

40. Han B, Xu XG, Chen GTY. Proton radiography and fluoroscopy of lung tumors: A Monte Carlo study using patient-specific 4DCT phantoms. Med Phys 2011; 38: 1903–1911. [PubMed: 21626923]

41. Maccabee HD, Madhvanath U, Raju MR. Tissue activation studies with alpha-particle beams. Phys Med Biol 1969; 14: 213–224 [PubMed: 5777096]

42. Llacer J, Chatterjee A, Alpen EL et al. Imaging by injection of accelerated radioactive particle beams. IEEE Trans Med Imaging 1984; 3: 80–90. [PubMed: 18234615]

43. Augusto R, Mendonca T, Wenander F et al. New developments of 11C post-accelerated beams for hadron therapy and imaging. Nucl Instrum Methods Phys Res B 2016; 376: 374–8.

44. Tobias CA, Benton EV, Capp MP et al. Particle radiography and autoactivation. Int J Radiat Oncol Biol Phys 1977; 3: 35–44. [PubMed: 614318]

45. Parodi K, Enghardt W and Haberer T. In-beam PET measurements of β+-radioactivity induced by proton beams. Phys Med Biol 2002; 47: 21–36. [PubMed: 11814225]

46. Priegnitz M, Möckel D, Parodi K et al. In-beam PET measurement of 7Li3+ irradiation induced β +-activity. Phys Med Biol 2008; 53: 4443–53. [PubMed: 18670054]

47. Pawelke J, Byars L, Enghardt W et al. The investigation of different cameras for in-beam PET imaging. Phys Med Biol1996; 41: 279–296. [PubMed: 8746110]

48. Nishio T, Miyatake A, Ogino T et al. The Development and Clinical Use of a Beam on-Line Pet System Mounted on a Rotating Gantry Port in Proton Therapy. Int J Radiat Oncol Biol Phys 2010; 76: 277–286. [PubMed: 20005459]

49. Zhu X, Espana S, Daartz J et al. Monitoring proton radiation therapy with in-room PET imaging. Phys Med Biol 2011; 56: 4041–4057. [PubMed: 21677366]

50. Vynckier S, Derreumaux S, Richard F et al. Is it possible to verify directly a proton-treatment plan using positron emission tomography?. Radiother Oncol 1993; 26: 275–277. [PubMed: 8391156]

51. Parodi K, Paganetti H, Shih HA et al. Patient study of in vivo verification of beam delivery and range, using positron emission tomography and computed tomography imaging after proton therapy. Int J Radiat Oncol Biol Phys 2017; 68: 920–34.

52. Ponisch F, Parodi K, Hasch B G and Enghardt W. The modelling of positron emitter production and PET imaging during carbon ion therapy. Phys Med Biol 2004; 49: 5217–32. [PubMed: 15656273]

53. Parodi K, Ferrari A, Sommerer F and Paganetti H. Clinical CT-based calculations of dose and positron emitter distributions in proton therapy using the FLUKA Monte Carlo code. Phys Med Biol 2007; 52: 3369–87. [PubMed: 17664549]

54. Kraan AC. Range verification methods in particle therapy: underlying physics and Monte Carlo modeling. Front Oncol 2015; 5: 150. [PubMed: 26217586]

55. Miyatake A, Nishio T and Ogino T. Development of activity pencil beam algorithm using measured distribution data of positron emitter nuclei generated by proton irradiation of targets containing (12)C, (16)O, and (40)Ca nuclei in preparation of clinical application. Med Phys 2011; 38: 5818–29. [PubMed: 21992396]

56. Frey K, Bauer J, Unholtz D et al. TPSPET-A TPS-based approach for in vivo dose verification with PET in proton therapy. Phys Med Biol 2014; 59: 1–21. [PubMed: 24323977]

57. Priegnitz M, Fiedler F, Kunath D et al. An Experiment-Based Approach for Predicting Positron Emitter Distributions Produced During Therapeutic Ion Irradiation. IEEE Trans Nucl Sci 2012; 59: 77–87.

58. Enghardt W, Parodi K, Crespo P et al. Dose quantification from in-beam positron emission tomography. Radiother Oncol 2004; 73(Suppl 2): S96–98. [PubMed: 15971319]

59. Bauer J, Unholtz D, Sommerer F et al. Implementation and initial clinical experience of offline PET/CT-based verification of scanned carbon ion treatment. Radiother Oncol 2013; 107: 218–226. [PubMed: 23647759]

60. Min CH, Zhu X, Winey BA et al. Clinical Application of In-Room Positron Emission Tomography for In Vivo Treatment Monitoring in Proton Radiation Therapy. Int J Radiat Oncol Biol Phys 2013; 86: 183–9. [PubMed: 23391817]

61. Kurz C, Bauer J, Unholtz D et al. Initial clinical evaluation of PET-based ion beam therapy monitoring under consideration of organ motion. Med Phys 2016; 43: 975–982. [PubMed: 26843257]

62. Handrack T Tessonnier W. Chen et al. Sensitivity of post treatment positron-emission-tomography/ computed-tomography to detect inter-fractional range variations in scanned ion beam therapy. Acta Oncol 2017; 56:1451–1458. [PubMed: 28918686]

63. Frey K, Unholtz D, Bauer J et al. Automation and uncertainty analysis of a method for in vivo range verification. in particle therapy. Phys Med Biol 2014; 59: 5903–5919. [PubMed: 25211629]

64. Nischwitz SP, Bauer J, Welzel T, Rief H, Jäkel O, Haberer T, Frey K, Debus J, Parodi K, Combs SE, Rieken S. Clinical implementation and range evaluation of in vivo PET dosimetry for particle irradiation in patients with primary glioma. Radiother Oncol.l 2015; 115: 179–8563

65. Bisogni MG, Attili A, Battistoni G et al. INSIDE in-beam positron emission tomography system for particle range monitoring in hadrontherapy. J med imag 2017; 4**:** 011005.**:**

66. Yamaya T, Yoshida E, Inaniwa T et al. Development of a small prototype for a proof-of concept of OpenPET imaging. Phys Med Biol 2011; 56: 1123–37. [PubMed: 21263176]

67. Tashima H, Yamaya T, Yoshida E et al. A single-ring OpenPET enabling PET imaging during radiotherapy. Phys Med Biol 2012; 57: 4705–18. [PubMed: 22750792]

68. Tashima H, Yoshida E, Inadama N et al. Development of a small single-ring OpenPET prototype with a novel transformable architecture. Phys Med Biol 2016; 61:1795–809. [PubMed: 26854528]

69. Sportelli G, Belcari N, Camarlinghi N et al. First full-beam PET acquisitions in proton therapy with a modular dual-head dedicated system. Phys Med Biol 2014; 59: 43–60. [PubMed: 24321855]

70. Helmbrecht S, Enghardt W, Fiedler F et al. In-beam PET at clinical proton beams with pile-up rejection. Z Med Phys 2017; 27:202–217. [PubMed: 27550545]

71. Crespo P, Shakirin G, Fiedler F et al. Direct time-of-flight for quantitative, real-time in-beam PET: a concept and feasibility study. Phys Med Biol 2007; 52: 6795–6811. [PubMed: 18029976]

72. Buitenhuis HJT, Diblen F, Brzezinski KW et al. Beam-on imaging of short-lived positron emitters during proton therapy. Phys Med Biol 2017; 62: 4654–4672. [PubMed: 28379155]

73. Stichelbaut F, Jongen Y, presented at the PTCOG 39, San Fransisco, 2003.

74. Min CH, Kim CH, Youn M, Kim J, Prompt Gamma Measurements for Locating Dose falloff Region in Proton Therapy, App. Phys. Lett 2006; 89, 183517.

75. Testa E, Bajard M, Chevallier M, Dauvergne D, Le Foulher F, Freud N, Poizat JC, Ray C, Testa M, Monitoring the Bragg peak location of 73 MeV/u carbon ions by means of prompt gamm ray measurements, App Phys Lett 2008; 93, 093506.

76. Moteabbed M, Espana S, Paganetti H, Monte Carlo patient study on the comparison of prompt gamma and PET imaging for range verification in proton therapy, Phys. Med. Biol 2011; 56, 1063–1082. [PubMed: 21263174]

77. Polf J, Peterson S, Ciangaru G, Gillin M, Beddar S, Prompt gamma-ray emission from biological tissues during proton irradiation: a preliminary study, Phys Med Biol 2009; 54, 731–743. [PubMed: 19131673]

78. Bom V, Joulaeisadeh F, Beekman F, Real-time prompt gamma monitoring in spot-scanning proton therapy using imaging through a knife-edge-shaped slit, Phys Med Biol 2012; 57, 297–308. [PubMed: 22156148]

79. Cambraia Lopes P, Clementel E, Crespo P, Henrotin S, Huizenga J, Janssens G, Parodi K, Prieels D, Roellinghoff F, Smeets J, Stichelbaut F, Schaart DR, Time-resolved imaging of prompt-gamma rays for proton range verification using a knife-edge slit camera based on digital photon counters, Phys Med Biol 2015; 60, 6063–6085. [PubMed: 26216269]

80. Perali I, Celani A, Bombelli L, Fiorini C, Camera F, Clementel E, Henrotin S, Janssens G, Prieels D, Roellinghoff F, Smeets J, Stichelbaut F, Vander Stappen F, Prompt gamma imaging of proton pencil beams at clinical dose rate, Phys Med Biol 2014; 59, 5849–5871. [PubMed: 25207724]

81. Smeets J, Roellinghoff F, Prieels D, Stichelbaut F, Benilov A, Busca P, Fiorini C, Peloso R, Basilavecchia M, Frizzi T, Dehaes JC, Dubus A, Prompt gamma imaging with a slit camera for real-time range control in proton therapy, Phys Med Biol 2012; 57, 3371–3405. [PubMed: 22572603]

82. Priegnitz M, Barczyk S, Nenoff L, Golnik C, Keitz I, Werner T, Mein S, Smeets J, Vander Stappen F, Janssens G, Hotoiu L, Fiedler F, Prieels D, Enghardt W, Pausch G, Richter C, Towards clinical application: prompt gamma imaging of passively scattered proton fields with a knife-edge slit camera, Phys Med Biol 2016; 61, 7881–7905. [PubMed: 27779120]

83. Roellinghoff F, Benilov A, Dauvergne D, Dedes G, Freud N, Janssens G, Krimmer J, Letang JM, Pinto M, Prieels D, Ray C, Smeets J, Stichelbaut F, Testa E, Real-time proton beam range monitoring by means of prompt-gamma detection with a collimated camera, Phys Med Biol 2014; 59, 1327–1338. [PubMed: 24556873]

84. Testa E, Bajard M, Chevallier M, Dauvergne D, Le Foulher F, Freud N, Letang JM, Poizat JC, Ray C, Testa M, Dose profile monitoring with carbon ion beams by means of prompt-gamma measurements, Nucl. Intstrum. Methods Phys Res B 2009; 267, 993–996.

85. Richter C, Pausch G, Barczyk S, Priegnitz M, Keitz I, Thiele J, Smeets J, Vander Stappen F, Bombelli L, Fiorini C, Hotoiu L, Perali I, Prieels D, Enghardt W, Baumann M, First clinical application of a prompt gamma based in vivo proton range verification system, Radiother Oncol 2016; 118, 232–237. [PubMed: 26774764]

86. Xie Y, Bentefour EH, Janssens G, Smeets J, Vander Stappen F, Hotoiu L, Yin L, Dolney D, Avery S, O'Grady F, Prieels D, McDonough J, Solberg TD, Lustig RA, Lin A, Teo B-KK, Prompt Gamma Imaging for InVivo Range Verification of Pencil Beam Scanning Proton Therapy, Int J Radiat Oncol Biol Phys 2017; 99, 210–218. [PubMed: 28816148]

87. Verburg JM, Riley K, Bortfeld T, Seco J, Energy- and time-resolved detection of prompt gamma-rays for proton range verification, Phys Med Biol 2013; 58, L37–49. [PubMed: 24077338]

88. Golnik C, Hueso-Gonzalez F, Muller A, Dendooven P, Enghardt W, Fiedler F, Kormoll T, Roemer K, Petzoldt J, Wagner A, Pausch G, Range assessment in particle therapy based on prompt gamma-ray timing measurements, Phys Med Biol 2014; 59, 5399–5422. [PubMed: 25157685]

89. Verburg JM, Shih HA, Seco J, Simulation of prompt gamma-ray emission during proton radiotherapy, Phys Med Biol 2012; 57, 5459–5472. [PubMed: 22864267]

90. Verburg JM, Seco J, Proton range verification through prompt gamma-ray spectroscopy, Phys Med Biol 2014; 59, 7089–7106. [PubMed: 25365362]

91. Testa M, Min CH, Verburg JM, Schumann J, Lu HM, Paganetti H, Range verification of passively scattered proton beams based on prompt gamma time patterns, Phys Med Biol 2014; 59, 4181–4195. [PubMed: 25004257]

92. Verburg JM, Testa M, Seco J, Range verification of passively scattered proton beams using prompt gamma-ray detection, Phys Med Biol 2015; 60, 1019–1029. [PubMed: 25585521]

93. Hueso-Gonzalez F, Enghardt W, Fiedler F, Golnik C, Janssens G, Petzoldt J, Prieels D, Priegnitz M, Romer KE, Smeets J, Vander Stappen F, Wagner A, Pausch G, First test of the prompt gamma ray timing method with heterogeneous targets at a clinical proton therapy facility, Phys Med Biol 2015; 60, 6247–6272. [PubMed: 26237433]

94. Hueso-Gonzalez F, Fiedler F, Golnik C, Kormoll T, Pausch G, Petzoldt J, Romer KE, Enghardt W, Compton Camera and Prompt Gamma Ray Timing: Two Methods for In Vivo Range Assessment in Proton Therapy, Front Oncol 2016; 6, 80. [PubMed: 27148473]

95. Todd R, Nightengale J, Everett D, A proposed gamma camera, Nature 1974; 251, 132–134.

96. Frandes M, Zoglauer A, Maxim V, Prost R, A tracking Compton-scattering imaging system for hadrom therapy monitoring, IEEE Trans Nucl Sci 2010; 57, 144–150.

97. Kormoll T, Fiedler F, Schone S, Wustemann J, Zuber K, Enghardt W, Compton imager for in vivo dosimetry fo proton beams-a design study, Nucl Intstrum Methods Phys Res A 2011; 626–627, 114–119.

98. Richard MH, Chevallier M, Dauvergne D, Freud N, Henriquet P, Le Foulher F, Letang JM, Montarou G, Ray C, Roellinghoff E, Testa E, Testa M, Walenta AH, Design Guidelines for a Double Scattering Compton Camera for Prompt Imaging During Ion Beam Therapy: A Monte Carlo Simulation Study, IEEE Trans Nucl Sci 2011; 58, 87–94.

99. Roellinghoff F, Richard MH, Chevillier M, Constanzo M, Dauvergne D, Freud N, Henriquet P, Foulher F, Letang JM, Montarou G, Ray C, Testa E, Testa M, Walenta AH, Design of a Compton camera for 3D prompt gamma imaging during ion beam therapy, Nucl Intstrum Methods Phys Res A 2011; 648, s20–23.

100. Peterson SW, Roberts D, Polf JC, Optimizing a 3-stage Compton camera for measuring prompt gamma rays emitted during proton radiotherapy, Phys Med Biol 2010; 55, 6841–6856. [PubMed: 21048295]

101. Robertson D, Polf JC, Peterson S, Gillin M, Beddar S, Material efficiency studies for a Compton camera designed to measure characteristic prompt gamma rays emitted during proton beam radiotherapy, Phys Med Biol 2011; 56, 3047–3059. [PubMed: 21508442]

102. Ortega PG, Torres-Espallardo I, Cerutti F, Ferrari A, Gillam JE, Lacasta C, Llosa G, Oliver JF, Sala PR, Solevi P, Rafecas M, Noise evaluation of Compton camera imaging for proton therapy, Phys Med Biol 2015; 60, 1845–1863. [PubMed: 25658644]

103. Gillam JE, Torres-Espallardo I, Lacasta C, Llosa G, Barrio J, Stankova V, Solaz C, Rafecas M, Hodoscope Coincidence Imaging for Hadron Therapy Using a Compton Camera, Conference Records Nuclear Science Symposium and Medical Imaging Conference (NSS/MIC), 2011 IEEE2011; 4206–4210.

104. Kim CH, Park JH, Seo H, Lee HR, Gamma electron vertex imaging and application to beam range verification in proton therapy, Med Phys 2012; 39, 1001–1005. [PubMed: 22320809]

105. Kim CH, Park JH, Seo H, Lee HR, Erratum: Gamma electron vertex imaging and application to beam range verification in proton therapy. Med Phys 2012; 39: 6523–6524 [PubMed: 28525152]

106. Krimmer J, Dauvergne D, Letang JM, Testa E, Prompt-gamma monitoring in hadrontherapy: A review, Nucl Intstr Met Phys Res A 2018; 878, 58–73.

107. Krimmer J, Ley JL, Abellan C, Cachemiche JP, Caponetto L, Chen X, Dahoumane M, Dauyergne D, Freud N, Joly B, Lambert D, Lestand L, Letang JM, Magne M, Mathez H, Maxim V, Montarou G, Morel C, Pinto M, Ray C, Reithinger V, Testa E, Zoccarato Y, Development of a Compton camera for medical applications based on silicon strip and scintillation detectors, Nucl Instrum Meth A 2015; 787, 98–101.

108. Gillam JE, Lacasta C, Torres-Espallardo I, Candela J, Llosa G, Solevi P, Barrio J, Rafecas M, A Compton imaging algorithm for on-line monitoring in hadron therapy, Proc. SPIE 7961, Medical Imaging 2011: Physics of Medical Imaging2011.

109. Mackin D, Peterson S, Beddar S, Polf J, Evaluation of a stochastic reconstruction algorithm for use in Compton camera imaging and beam range verification from secondary gamma emission during proton therapy, Phys Med Biol 2012; 57, 3537–3553. [PubMed: 22588144]

110. Draeger E, Peterson S, Mackin D, Chen H, Beddar S, Polf JC, Feasibility Studies of a New Event Selection Method to Improve Spatial Resolution of Compton Imaging for Medical Applications, IEEE T Rad Plasma Med Sci 2017; 1, 358–367.

111. Hueso-Gonzalez F, Pausch G, Petzoldt J, Romer KE, Enghardt W, Prompt Gamma Rays Detected With a BGO Block Compton Camera Reveal Range Deviations of Therapeutic Proton Beams, IEEE TRPMS 2017; 1, 76–86.

112. Polf J, Avery S, Mackin D, Beddar S, Imaging of prompt gamma rays emitted during delivery of clinical proton beams with a Compton camera: feasibility studies for range verification, Phys Med Biol 2015; 16, 7085–7099.

113. Solevi P, Munoz E, Solaz C, Trovato M, Dendooven P, Gillam JE, Lacasta C, Oliver JF, Rafecas M, Torres-Espallardo I, Llosa G, Performance of MACACO Compton telescope for ion-beam therapy monitoring: first test with proton beams, Phys. Med. Biol 2016; 61, 5149–5165. [PubMed: 27352107]

114. Draeger E, Mackin D, Peterson S, Chen H, Avery S, Beddar S, Polf JC, 3D prompt gamma imaging for proton beam range verification, Phys Med Biol 2018; 63, 035019. [PubMed: 29380750]

115. Mackin D, Polf J, Peterson S, Beddar S, The effects of Doppler broadening and detector resolution on the performance of three-stage Compton cameras, Med Phys 2013; 40, 012402. [PubMed: 23298111]

116. Kohno R, Hotta K, Matsubara K, Nishioka S, Matsuura T, Kawashima M, In vivo proton dosimetry using a MOSFET detector in an anthropomorphic phantom with tissue inhomogeneity, J Appl Clin Med Phys 2012; 13, 3699 [PubMed: 22402385]

117. Lu H-M, Mann G, Cascio E, Investigation of an implantable dosimeter for single-point water equivalent path length verification in proton therapy, Med Phys 2010; 37, 5858–5866. [PubMed: 21158298]

118. Cho J, Ibbot G, Gillin M et al. Feasibility of proton-activated implantable markers for proton range verification using PET. Phys Med Biol 2013; 58: 7497–7512. [PubMed: 24099853]

119. Tang S, Both S, Bentefour H et al. Improvement of prostate treatment by anterior proton fields. Int J Radiat Oncol Biol Phys 2012; 83: 408–418. [PubMed: 22133626]

120. Bentefour EH, Tang S, Cascio EW et al. Validation of an in-vivo proton beam range check method in an anthropomorphic pelvic phantom using dose measurements. Med Phys 2015; 42: 1936–1947. [PubMed: 25832084]

121. Toltz A, Hoesl M, Schuemann J, Seuntjens J, Lu HM, Paganetti H. Time-resolved diode dosimetry calibration through Monte Carlo modeling for in vivo passive scattered proton therapy range verification. J Appl Clin Med Phys 2017; 18:200–205

122. Hoesl M, Deepak S, Moteabbed M, Jassens G, Orban J, Park YK, Parodi K, Bentefour EH, Lu HM. Clinical commissioning of an in vivo range verification system for prostate cancer treatment with anterior and anterior oblique proton beams Phys Med Biol 2016; 61:3049–62 [PubMed: 27002470]

123. Gensheimer MF, Yoock TI, Liebsch NJ et al. In Vivo Proton Beam Range Verification Using Spine MRI Changes. Int J Radiat Oncol Biol Phys 2010; 78: 268–275. [PubMed: 20472369]

124. Yuan Y, Andronesi OC, Bortfeld TR et al. Feasibility study of in vivo MRI based dosimetric verification of proton end-of-range for liver cancer patients. Radiother Oncol 2013; 106: 378–382 [PubMed: 23473960]

125. Hayakawa Y, Tada J, Arai N et al. Acoustic pulse generated in a patient during treatment by pulsed proton radiation beam. Radiat Oncol Investig 1995; 3: 42–45.

126. Assmann W, Kellnberger S, Reinhardt S et al. Ionoacoustic characterization of the proton Bragg peak with submillimeter accuracy. Med Phys 2015; 42: 567–574. [PubMed: 25652477]

127. Jones KC, Seghal CM, S. Avery. How proton pulse characteristics influence protoacoustic determination of proton-beam range: simulation studies. Phys Med Biol 2016; 61: 2213–2242. [PubMed: 26913839]

128. Lehrack S, Assmann W, Bertrand D et al. Submillimeter ionoacoustic range determination for protons in water at a clinical synchrocyclotron. Phys Med Biol 2017; 62: L20–L30. [PubMed: 28742053]

129. Jones KC, Vander Stappen F et al. Experimental observation of acoustic emissions generated by a pulsed proton beam from a hospital-based clinical cyclotron. Med Phys 2015; 42: 7090–7 [PubMed: 26632062]

130. Jones KC, Nie W, Chu JCH et al. Acoustic-based proton range verification in heterogeneous tissue: simulation studies. Phys Med Biol 2018;63:025018 [PubMed: 29176057]

131. Patch SK, Hoff DEM, Webb TB, Sobotka LG, Zhao T. Two-stage ionoacoustic range verification leveraging Monte Carlo and acoustic simulations to stably account for tissue inhomogeneity and accelerator-specific time structure - A simulation study. Med Phys 2018;45:783–793 [PubMed: 29159885]

132. Kellnberger S, Assmann W, Lehrack S et al. Ionoacoustic tomography of the proton Bragg peak in combination with ultrasound and optoacoustic imaging. Sci Rep 2016; 6: 29305. [PubMed: 27384505]

133. Patch SK, Kireeff Covo M, Jackson A et al. Thermoacoustic range verification using a clinical ultrasound array provides perfectly co-registered overlay of the Bragg peak onto an ultrasound image. Phys Med Biol 2016; 61: 5621–38 [PubMed: 27385261]

134. Parodi K. On- and off-line monitoring of ion beam treatment. Nucl Instrum Methods Phys Res A 2016; 809: 113–9

135. Dyer P, Bodansky D, Seamster AG et al. Cross sections relevant to gamma-ray astronomy: Proton induced reactions. Phys Rev C 1981; 23: 1865–1882.

136. Kiener J, Berheide M, Achouri NL et al. Gamma ray production by inelastic proton scattering on 16O and 12C. Phys Rev C 1998; 28: 2174–2179.

137. Polf JC, Peterson S, McCleskey M et al. Measurement and calculation of characterisitic prompt gamma ray spectra emitted during proton irradiation. Phys Med Biol 2009; 54: N519–N527. [PubMed: 19864704]

138. Polf JC, Panthi R, Mackin RS et al. Measurement of characteristic prompt gamma rays emitted from oxygen and carbon in tissue-equivalent samples during proton beam irradiation. Phys Med Biol 2013; 58: 5821–5831. [PubMed: 23920051]

139. Oborn BM, Dowdell S, Metcalfe PE et al. Future of medical physics: Real-time MRI-guided proton therapy. Med Phys 2017; 44: e77–e90 [PubMed: 28547820]
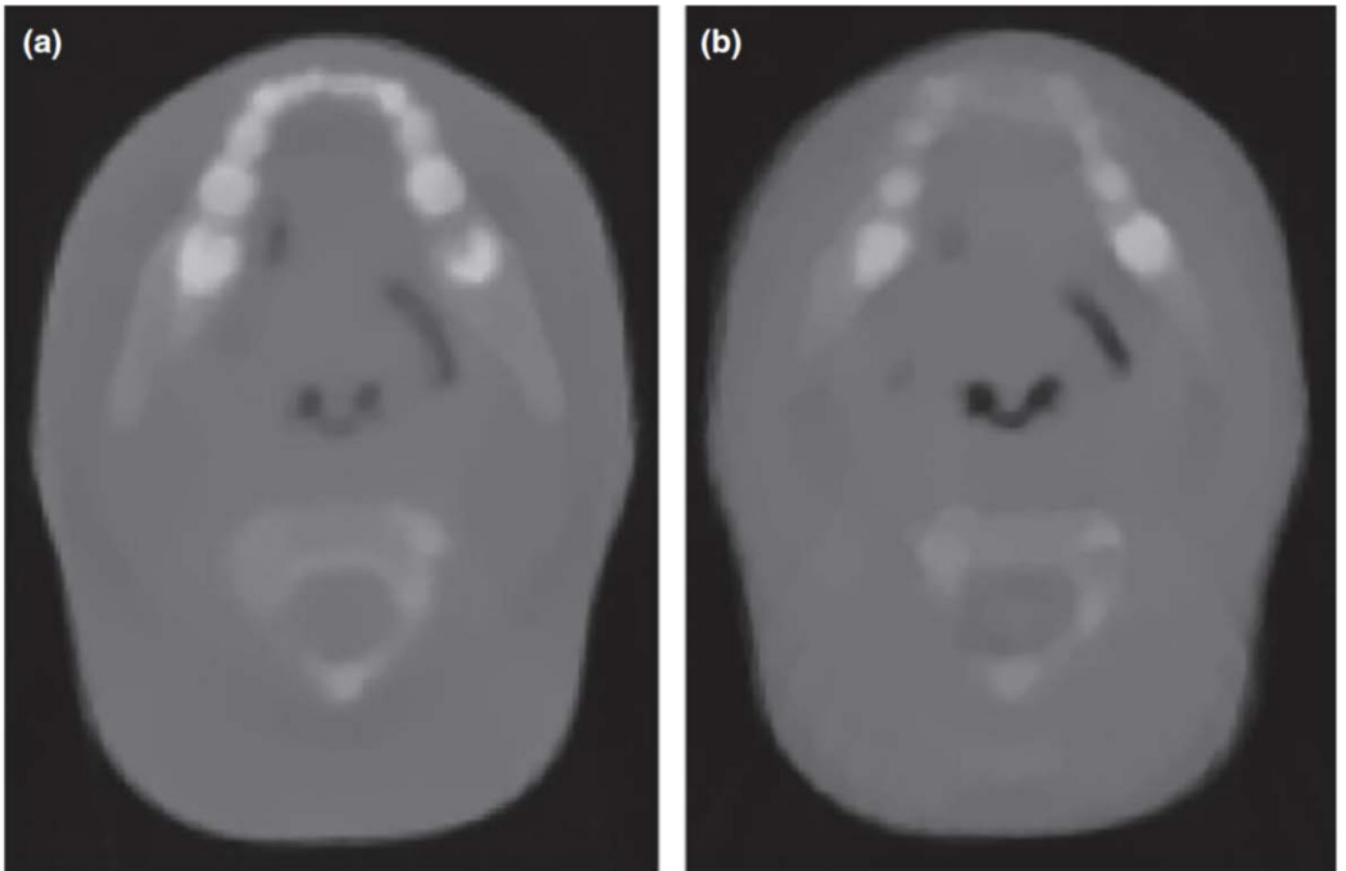
Figure 1:

Example of instrumentation for proton/ion radiography and tomography, featuring a) silicon-based trackers followed by a multi-stage calorimeter for single proton imaging of a passively scattered monoenergetic broad beam[19], b) a range telescope made by large area plane-parallel ionization chambers interleaved with plastic degraders for imaging of scanned carbon ion beams[15] and c) a matrix of diodes combined with a passively energy modulated broad proton beam[24]. Adapted with permission.

Figure 2:
Reconstructed proton computed tomography images from experimental (a) and simulated (b)
projections acquired for a pediatric head phantom with the prototype scanner shown in
figure 1a. The selected slice is approximately taken at the same anatomical position. Figure
from Giacometti et al[30], with permission.

Figure 3:
Example of PET instrumentation already used for clinical studies, featuring (a) an on-board planar system integrated in a proton gantry for imaging immediately after end of treatment[48], (b) a neurological PET scanner on-wheel for in-room imaging few minutes after end of treatment[49,60], and (c) a commercial PET/CT scanner for offline imaging several minutes after end of treatment[59], with permission.
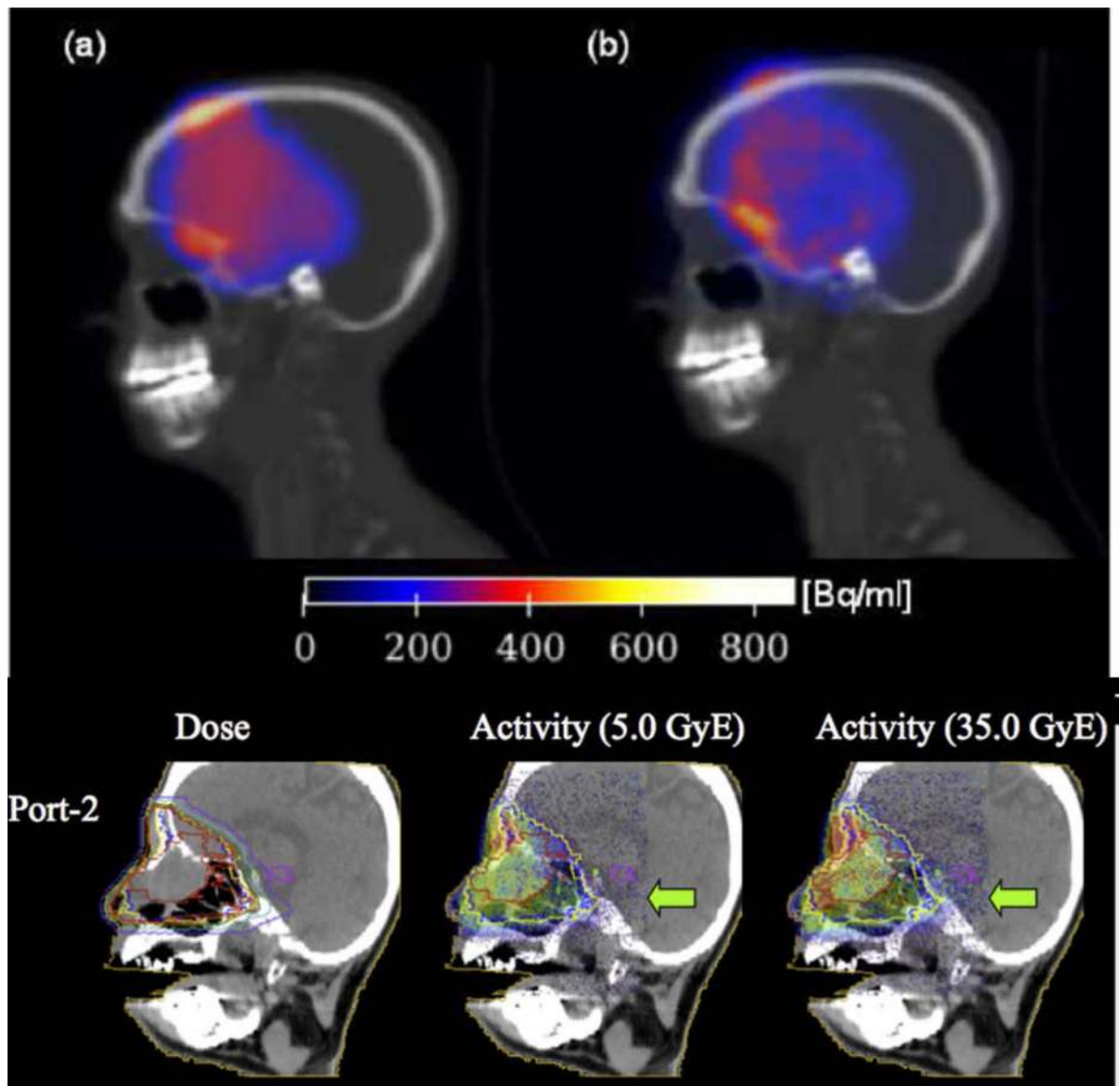
Figure 4:
Example of PET monitoring of passively scattered proton therapy with fraction doses of 1,8 – 2,5 GyE (RBE 1.1) and imaging starting 140s (top) and immediately after (bottom) irradiation for a scan time of 1200s and 200s, respectively (with permission). Top panel: comparison between simulated (a) and measured (b) activity[63] using the in-room PET scanner shown in figure 3b[49]. Bottom panel: comparison between the planned dose distribution for the considered second port (left) and the activity measured with the on-board planar detector of figure 3a at two different treatment fractions, corresponding to the total delivery of a biologically weighted dose of 5 GyE (middle) and 35 GyE (right). The green arrow marks regions of disagreement, indicating a later radiologically confirmed anatomical change[48].
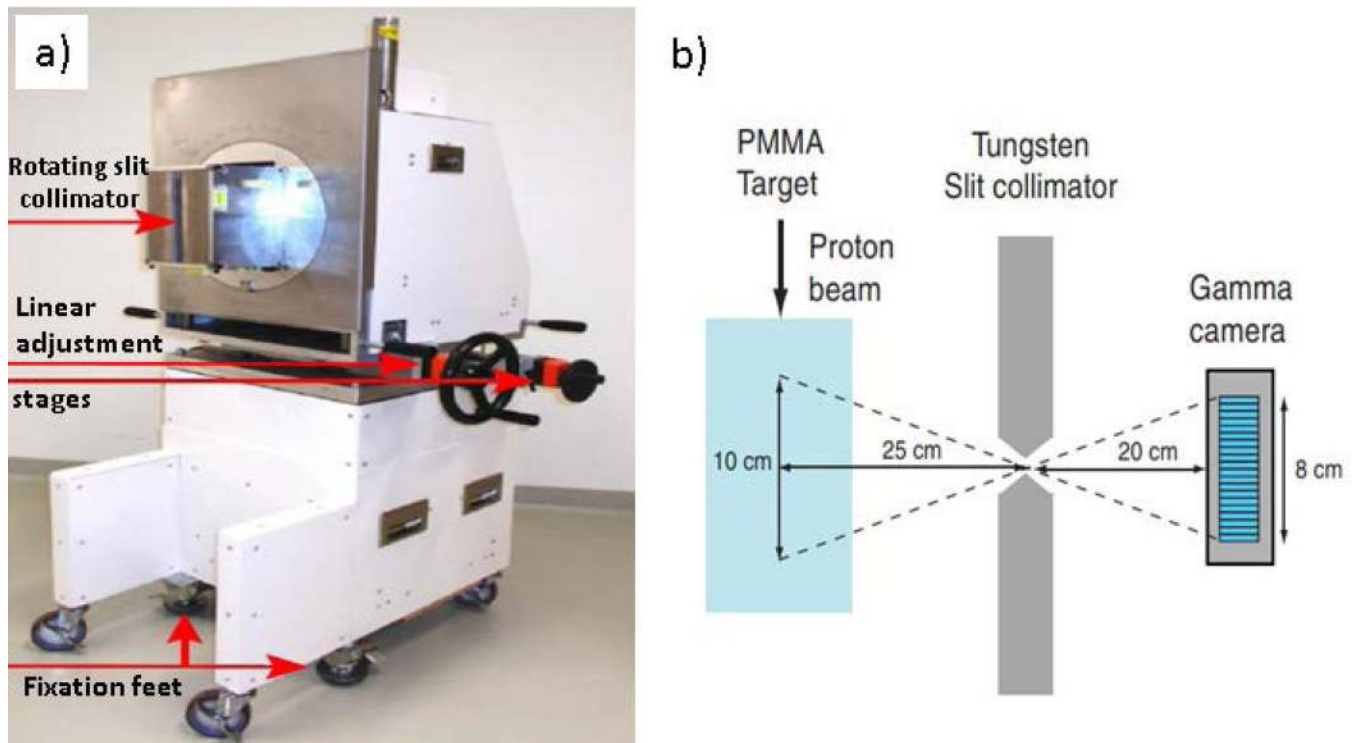
Figure 5:
a) The clinical slit-camera used for patient range verification (adapted from Richter et al[85]), as well as b) a schematic drawing of the slit-collimator imaging concept in which the originating position of the PG is derived from the vector connecting its point of detection in the camera and the opening of the collimator (adapted from Perali et al[80]), with permission.
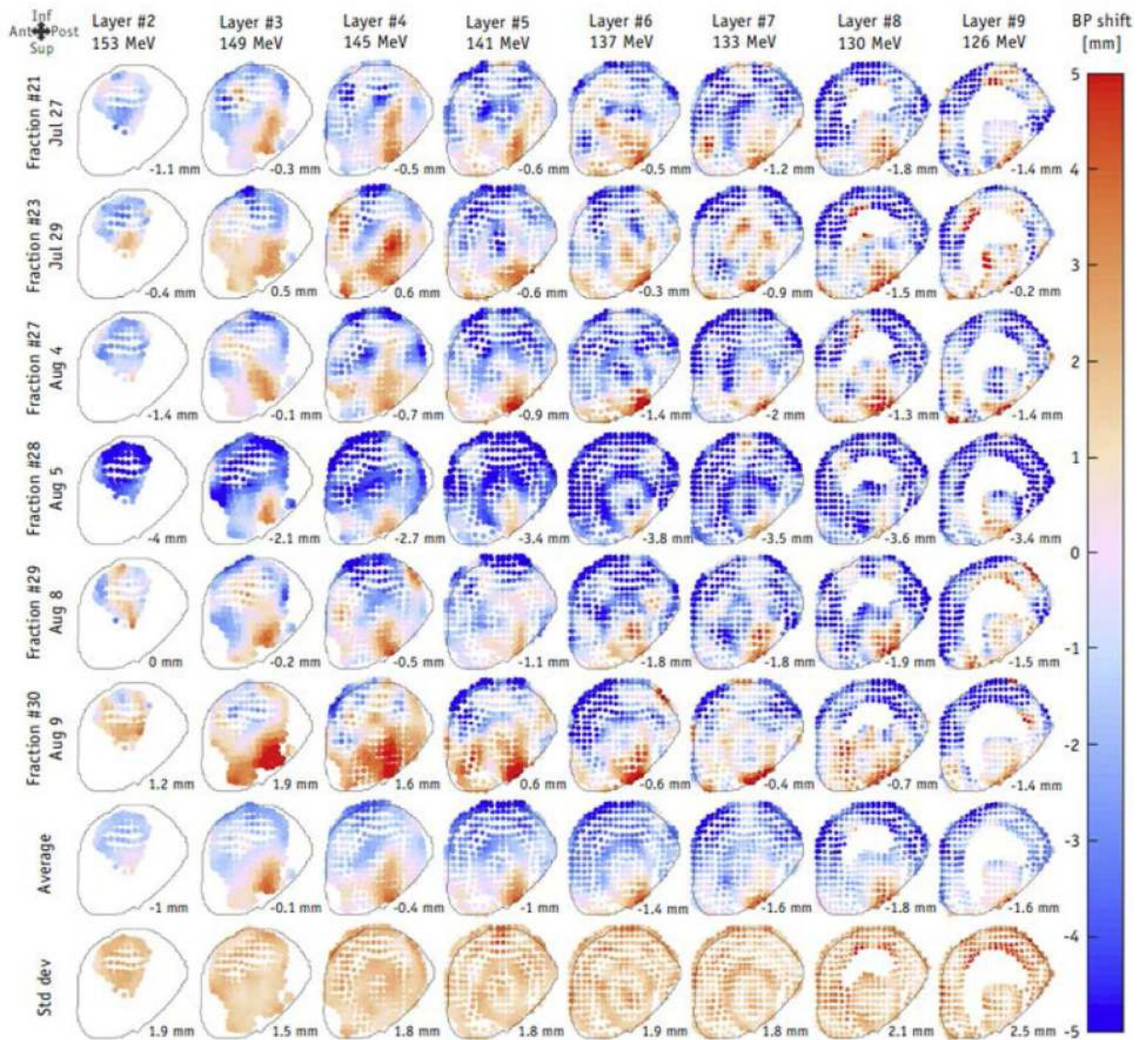
Figure 6:
Range shift maps for individual beam spots for a single treatment field delivered for six different fractions measured with a clinical slit camera. Each map show the deviation of the measured range from the planned range for each spot in each energy layer of the treatment field (from Xie et al[86] with permission)
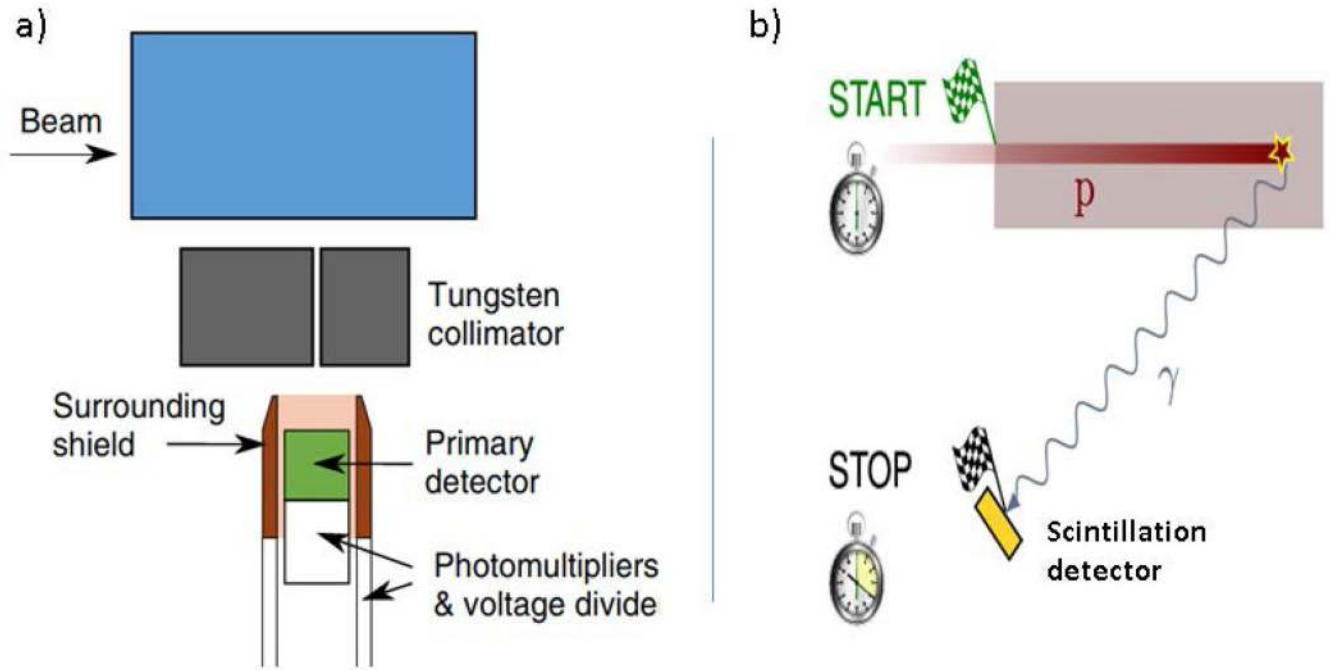
Figure 7:
Schematic drawing of a) an energy-time resolved prompt gamma spectroscopy system containing a collimated scintillator enclosed within a Compton scattered suppression shield (adapted from Verburg et al[90] with permission). b) A schematic of the prompt gamma timing concept in which the beam range is derived from the measurement of the time elapsed between the start a proton beam pulse and the arrival of a prompt gamma ray at the scintillation detector (adapted from Hueso-Gonzalez et al[94] in accordance with CC BY license agreement).
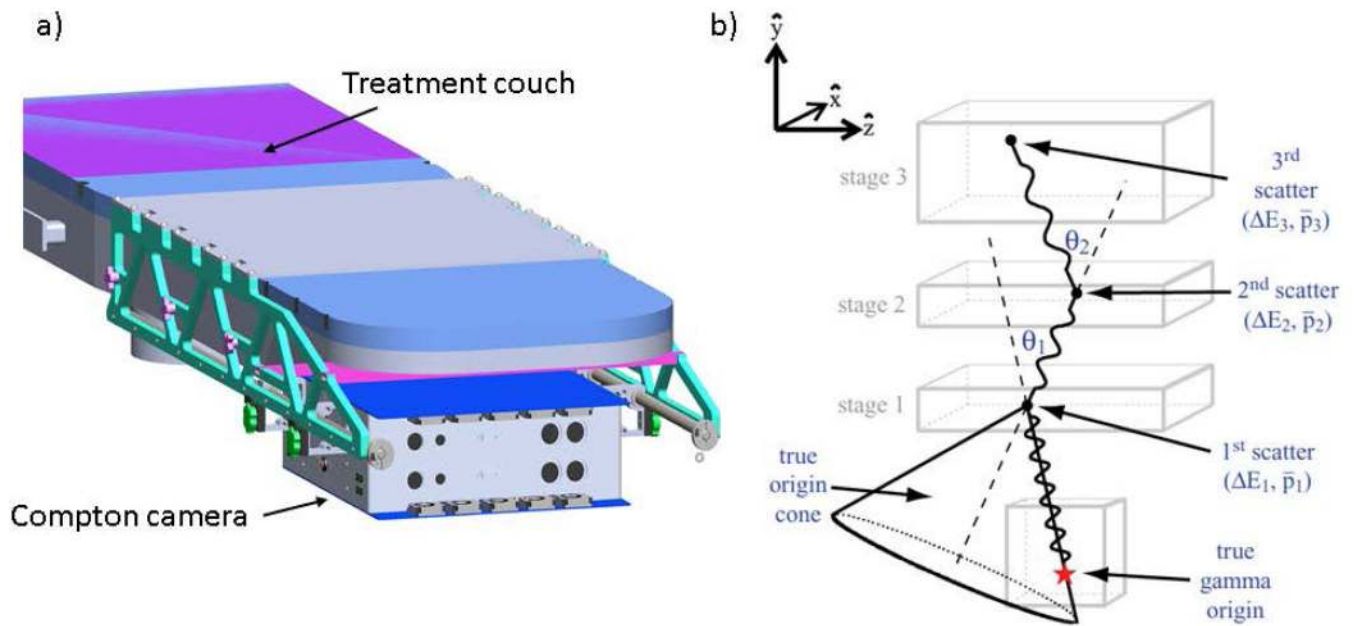
Figure 8:
Schematic drawing of a) a clinical Compton camera based range verification system with the CC mounted on a rail system attached to the patient treatment couch for setup and positioning. b) schematic of a CC showing multiple PG scatters used to create the "cone-of-origin" (adapted from Mackin et al[115] with permission).
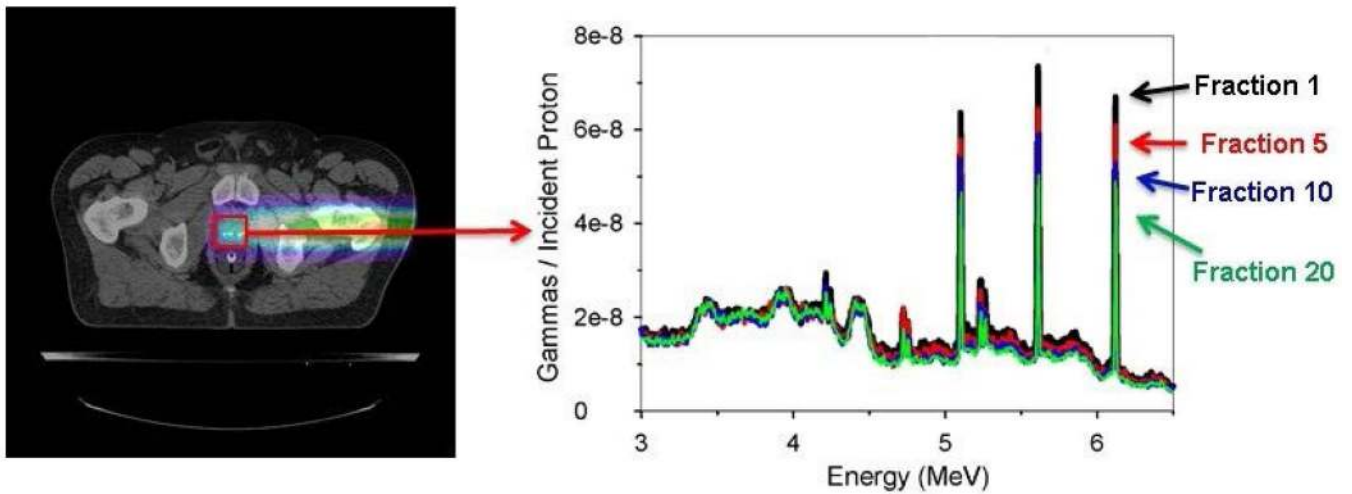
Figure 9:
Illustration of spectroscopic PG imaging in proton or heavy ion therapy. The image is reconstructed from PGs emitted during delivery of a daily treatment fraction. The PG spectra formed within a specific region of interest (ROI) can then be constructed. Comparison of changes in the relative intensity of PG emission lines from specific elements (6.12 MeV emission from ^{16}O highlighted) in the ROI spectra over the course of treatment could potentially be used to infer how the concentration of different elements are changing in response to the treatment (adapted from Polf et al[138] with permission).